

Journal of
Mechanics of
Materials and Structures

**COMPARATIVE STUDY OF SYMMETRIC AND ASYMMETRIC
DEFORMATION OF AL SINGLE CRYSTAL UNDER MICROSCALE
LASER SHOCK PEENING**

Siniša Vukelić, Youneng Wang, Jeffrey W. Kysar and Y. Lawrence Yao

Volume 4, N° 1

January 2009



mathematical sciences publishers

COMPARATIVE STUDY OF SYMMETRIC AND ASYMMETRIC DEFORMATION OF AL SINGLE CRYSTAL UNDER MICROSCALE LASER SHOCK PEENING

SINIŠA VUKELIĆ, YOUNENG WANG, JEFFREY W. KYSAR AND Y. LAWRENCE YAO

The process of laser shock peening induces compressive residual stresses in a material to improve material fatigue life. For micron sized laser beams, the size of the laser-target interaction zone is of the same order of magnitude as the target material grains and, thus, the target material must be considered anisotropic and inhomogeneous. Single crystals are chosen to study the effects of the anisotropic mechanical properties. It is of further interest to investigate the response of symmetric and asymmetric slip systems with respect to the shocked surface. In the present study, analytic, numerical, and experimental aspects of laser shock peening on two different crystal surfaces, (110) and (1 $\bar{1}$ 4), of aluminum single crystals are studied. Anisotropic slip line theory is employed for the construction of slip line fields for both orientations and compared with numerical results. Lattice rotations of the cross section are measured using Electron Backscatter Diffraction (EBSD).

1. Introduction

Laser shock peening (LSP) is a surface treatment introduced in the 1960s [Clauer and Holbrook 1981; Fabbro et al. 1990; Clauer and Lahrman 2001] as a potential replacement for shot peening, which has the same goal of inducing compressive residual stresses on the surface of a material to improve fatigue behavior and wear resistance of the target material. Shocks induced by a laser induce compressive residual stresses of the same order of magnitude as those created by conventional shock peening, however, the residual stresses generated by LSP penetrate deeper into the material resulting in the significant improvement of material response to the cyclic loading [Hammersley et al. 2000]. Moreover, it is much easier to control the position of laser beams, and the process as a whole is much more flexible.

More recently, microscale laser shock peening (μ LSP) has been employed as a means to improve reliability of various micro devices, such as MEMS (microelectromechanical systems). The process is performed by coating the specimen with an ablative layer and submerging it into water, after which a high intensity laser is directed at the ablative layer for 50 ns. The result is a plasma confined by the surrounding fluid so that much of the energy is directed into the material as a shock pulse. The process is considered to be primarily mechanical without any thermal effects that modify the microstructure. Most of the initial work in this field was on polycrystalline materials [Zhang and Yao 2002; Fan et al. 2005].

Keywords: laser shock peening, single crystal, micromechanics, anisotropic slip line theory.

This work is supported by National Science Foundation under grant DMII-0500239. Dr. Jean Jordan Sweet of IBM Watson Research Center provided help with usage of X-ray microdiffraction equipment at the National Synchrotron Light Source at Brookhaven National Laboratory. This work has used the shared experimental facilities that are supported primarily by the MRSEC Program of the National Science Foundation under Award Number DMR – 0213574 by the New York State Office of Science, Technology and Academic Research (NYSTAR). Dr. Paul van der Wilt generously assisted during EBSD measurements.

However, since the laser beam spot size, usually several microns, is comparable to the average grain size of most polycrystalline materials used in the fabrication of microdevices (aluminum, copper, etc.), at most a few grains are affected by a single laser pulse. Thus the effects of anisotropy and heterogeneity have to be taken into account to properly understand this process. This was the motivation for previous studies [Chen et al. 2004a] in which the response of single crystals of aluminum and copper were examined after laser treatment. Two different orientations of aluminum and copper single crystals were examined, a numerical model was established, and the results were compared to experimental findings.

Anisotropic properties of single crystal materials have been studied extensively. One of the early efforts was presented by Hill [1998], who extended the classical slip line theory [Hencky 1923] developed for isotropic materials by substituting a circular yield surface with an elliptic one. Rice [1973] and Booker and Davis [1972] went further in the generalization of slip line theory by expanding it to materials with arbitrary anisotropy. Asaro [1983] summarized the principles of single crystal plasticity. Anisotropic slip line theory as well as plasticity theory was applied to the problem of a flat punch impinged onto the surface of a plastic medium of arbitrary anisotropy [Rice 1973]. The same theory was used by Rice [1987] and Dragan [2001] for derivation of the asymptotic crack tip stress field solutions for elastic ideally-plastic single crystals. An analytic solution for the stress distribution and deformation state around a cylindrical void has been found in [Kysar 1997; 2001a; 2001b].

Single crystal plasticity and anisotropic slip line theory have also been employed to study the response of single crystals under laser shock peening. The approach taken by Wang et al. [2008] was to approximate the Gaussian pressure loading from laser shocks as a punch problem with nonuniform pressure. An aluminum single crystal of a nonsymmetric ($\bar{1}\bar{1}4$) orientation was used in the study because only one slip system was predicted to be active directly under the applied loading. The size of the deformed region was estimated, and an approximate analytic solution was obtained and compared with findings acquired from numerical analysis.

A symmetric orientation of the crystal is of interest because multiple slip systems are activated under a Gaussian pressure distribution. This complicates the analytic derivation and raises issues of the difference in material response and stress field distributions between nonsymmetric and symmetric cases. In the present study, the (110) orientation is chosen because two slip systems are activated under loading, since the symmetry of the yield surface simplifies the derivation of the deformation field. Furthermore, in real applications, polycrystalline materials with textures involving mostly low Miller index grains are quite common.

Thus, the objective of this work is a comparative study of aluminum single crystal behavior under a Gaussian pressure distribution induced by μ LSP for two different crystallographic surfaces, one nonsymmetric with high Miller index ($\bar{1}\bar{1}4$) and the other symmetric with low Miller index (110). A line of μ LSP shocks exists in the ($\bar{1}\bar{1}0$) on the respective surfaces in order to introduce an approximate two-dimensional deformation state. The effects of anisotropy are emphasized, neglecting inertial terms present due to the dynamic nature of the process, terms which are taken into account in [Vukelic et al. \geq 2009]. The deformation state is characterized experimentally, and anisotropic slip line theory is used to investigate the stress distribution and deformation state induced by laser shock peening of a single crystal surface under plane strain conditions. In addition, the finite element method (FEM) is used for the detailed analysis of single crystal plasticity as another perspective of the study. The results are clearly approximate because inertia is neglected, however, the results give insight into the role of anisotropy.

2. Experimental setup and characterization

Twelve dislocation-mediated plastic slip systems exist in the face-centered cubic aluminum, denoted as $\{111\} \langle 110 \rangle$, where $\{111\}$ corresponds to the family of slip planes and $\langle 110 \rangle$ denotes the family of slip directions. If a line loading is applied parallel to the $(\bar{1}10)$ direction, the twelve physical slip systems reduce to three effective in-plane slip systems resulting in an approximate plane strain deformation [Rice 1973; 1987; Kysar et al. 2005]. Lines of laser shocks applied parallel to the $(\bar{1}10)$ direction on the (110) and $(1\bar{1}4)$ planes are called, respectively, the symmetric and asymmetric deformations. The symmetric case admits slip on two effective in-plane slip systems in the region immediately below the laser shock. The asymmetric case admits slip only on one effective slip system. The two experimental setups with effective in-plane slip systems are shown in Figure 1. A detailed discussion about the formation of the approximate two-dimensional deformation can be found in [Rice 1987; Kysar 2001a; Kysar et al. 2005]. The geometric conditions needed for plane strain conditions to be achieved are summarize in [Crone et al. 2004].

Aluminum single crystals are used in this study grown via the Bridgeman method. The sample is mounted on a three circle goniometer and its orientation is determined by Laue diffraction. The specimen is cut to size with a wire electrical discharge machine (EDM) to within $\pm 1^\circ$ of the desired orientation, and the resulting heat affected zone (HAZ) is removed via mechanical polishing. Finally, electropolishing is used in order to remove any residual deformed material.

A frequency tripled Q-switched Nd:YAG laser with wavelength $\lambda = 355$ nm in TEM₀₀ mode is used for the μ LSP experiments, with a beam diameter of $12 \mu\text{m}$, pulse duration of 50 ns, and laser intensity of about 4 GW/cm^2 . A thin polycrystalline aluminum foil is used as an ablative coating applied tightly over an evenly spread layer (approximately $10 \mu\text{m}$ thick) of high vacuum grease. The specimen is placed into a shallow container filled with distilled water to about two millimeters above the sample's top surface as shown in Figure 1. More details about laser shocking can be found in [Zhang and Yao 2002; Chen et al. 2004b]. To obtain an approximate two-dimensional deformation state, laser shocks are applied with a $25 \mu\text{m}$ spacing along the $(\bar{1}\bar{1}0)$ direction.

μ LSP induces deformation into the single crystal that can be characterized experimentally through lattice rotation which is measured by comparing the as-deformed crystallographic orientation [Kysar 2001a; Wang et al. 2008] relative to the known undeformed state. Lattice orientation is measured using Electron Backscatter Diffraction (EBSD) as a function of micrometer scale spatial position. In order to get information about the depth of the affected region and magnitude of lattice rotation under the surface, EBSD mapping is employed on a cross section of the sample. For these measurements, an HKL Technology system attached to a JEOL JSM 5600LV scanning electron microscope (SEM) is used with a scan area of $200 \mu\text{m} \times 200 \mu\text{m}$ and $120 \mu\text{m} \times 120 \mu\text{m}$ on the shocked surface and cross section, respectively, with $3 \mu\text{m}$ step size.

3. Numerical simulation conditions of single crystals

Finite element analysis is performed based on single crystal plasticity theory described by [Asaro 1983]. For the purpose of this analysis, a plane strain model is established based upon results of prior experiments [Chen et al. 2004a; Wang et al. 2008; Vukelic et al. \geq 2009] which demonstrate that the deformation is approximately two-dimensional at any cross section along a shock line parallel to a $\langle 110 \rangle$ crystallographic

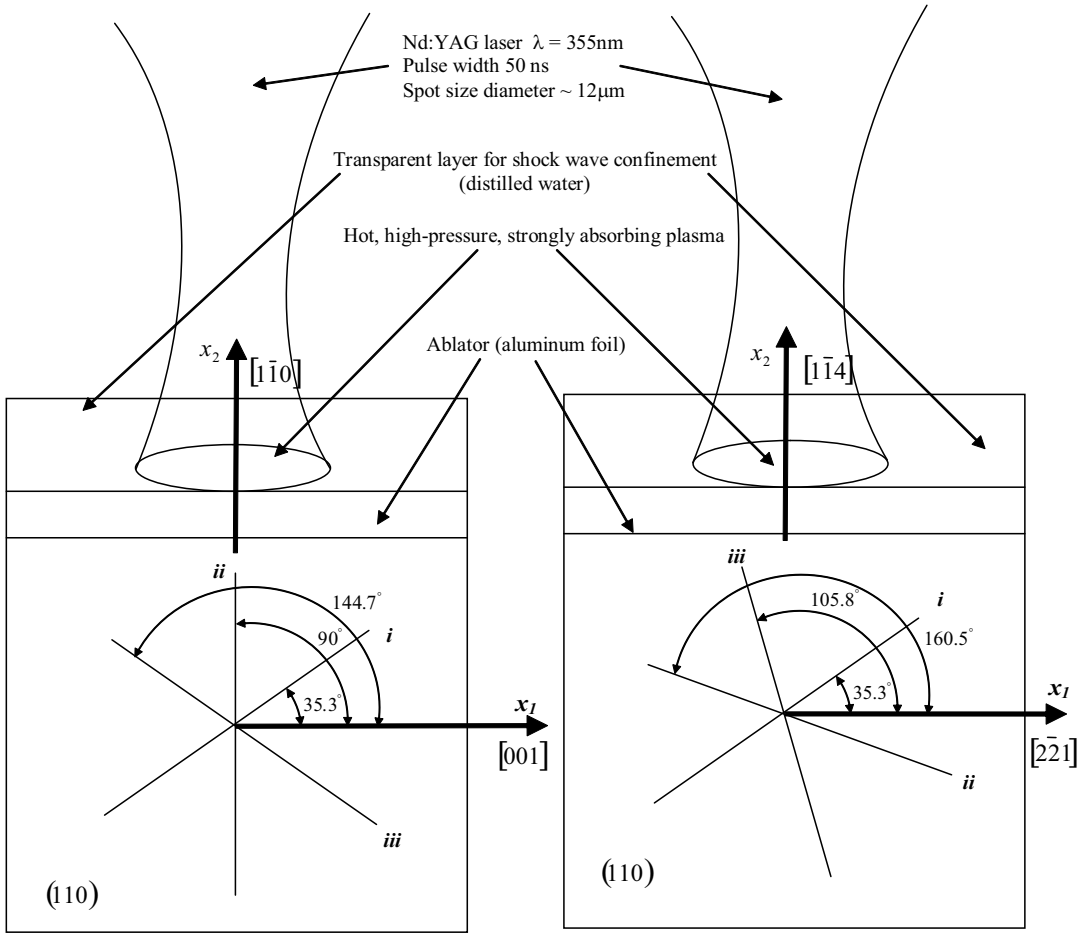


Figure 1. Experimental setup: effective in-plane strain slip systems active corresponding to the (110) orientation (left) and the $(1\bar{1}\bar{4})$ orientation (right).

direction. The simulation assumes quasistatic conditions, which, although a gross oversimplification in comparison to the highly dynamic character of μ LSP, still gives insight into the role of the anisotropy, especially in comparison to the analytic solution. Boundary conditions are specified, with reference to the configuration in Figure 1, as follows: zero traction on the side edges; zero vertical displacement on the bottom; and a Gaussian pressure distribution on the upper surface, given by

$$P(x) = P_0 \exp\left(-\frac{x^2}{2R^2}\right), \quad (1)$$

where R is the plasma radius, x is the distance from the center of the Gaussian pressure distribution and P_0 is the peak pressure. The analysis is performed with the commercial finite element (FEM) program ABAQUS/Standard with a user-defined material subroutine (UMAT) written by Huang [1991] and modified by Kysar [1997]. The aluminum slip systems are assumed to have a critical shear strength of $\tau \approx 1$ MPa; the peak pressure is taken to be $P_0/\tau = 7$.

4. Single crystal micromechanics

According to [Asaro 1983], plastic deformation of a single crystal can be conceptually broken down into three steps which, when combined, determine the overall deformation gradient F : first, plastic slip through the undeformed crystal F^P ; second, rigid body rotation F^R ; finally, elastic stretching of the lattice F^e . Therefore, the deformation gradient tensor can be multiplicatively decomposed as

$$F = F^e \cdot F^R \cdot F^P. \quad (2)$$

The first two terms of (2) can be combined together, and the general expression for the deformation gradient becomes $F = F^* \cdot F^P$, where F^P is the deformation related to the plastic shear and F^* represents the stretching and rotation of the crystal lattice. The velocity gradient, L , which is the sum of the spin rate tensor, Ω , and deformation rate tensor, D , can also be calculated as $L = \dot{F} \cdot F^{-1}$. Furthermore, D and Ω can be decomposed into $D = D^* + D^P$ and $\Omega = \Omega^* + \Omega^P$. It can then be shown that the constitutive equation in rate form is

$$\tau^\nabla = L : D - \sum_{\alpha=1}^n [L : P^{(\alpha)} + \beta^{(\alpha)}]_{\lambda}^{(\alpha)}, \quad (3)$$

where L is the tensor of elastic moduli, τ^∇ is the Jaumann rate of the Kirchhoff stress tensor, $\beta^{(\alpha)} = W^{(\alpha)} \dot{\tau} - \dot{\tau} W^{(\alpha)}$, and $\dot{\gamma}^{(\alpha)}$ is the shear strain rate on the slip system α . Another important issue is the definition of the Schmid stress, also known as resolved shear stress, which is responsible for producing an effective force on dislocations. From the general expression of the rate of work,

$$\tau : D^P = \sum_{\alpha=1}^n \tau : P_{\lambda}^{\alpha.(\alpha)}, \quad (4)$$

the Schmid stress on a particular slip system α is

$$\tau^{(\alpha)} = P^{(\alpha)} : \tau, \quad (5)$$

with the Schmid tensor defined as $P^{(\alpha)} = (n^{(\alpha)} \otimes s^{(\alpha)} + s^{(\alpha)} \otimes n^{(\alpha)})/2$, where $n^{(\alpha)}$ is the unit normal of the α -th {111} plane and $s^{(\alpha)}$ is the unit vector corresponding to the α -th <110> slip direction.

5. Anisotropic slip line theory

Slip line theory for isotropic rigid-ideally plastic materials experiencing plane strain deformation has been originally developed by Hencky [1923] and Prandtl [1923]. The stress distribution under a flat punch with a constant pressure was first derived by Hill [1998] for anisotropic materials with an elliptic yield surface using slip line theory and was solved with the generalized theory for arbitrary anisotropic yield surface by Rice [1973] and Booker and Davis [1972]. Wang et al. [2008] employed anisotropic slip line theory to investigate stress and deformation fields for the case of a Gaussian pressure distribution on a single crystal surface for the asymmetric case. In essence, they assumed that the deformation from μ LSP can be thought of as being induced by a punch with a Gaussian pressure distribution, rather than a constant pressure across the width of the punch.

Anisotropic slip line theory is employed to investigate the deformation field of a single face-centered cubic crystal under μ LSP for the symmetric case. Slip line theory treats incipient plane flow and it

is assumed that plastic deformation occurs simultaneously over the domain of interest. The governing equations are a set of equilibrium equations that have the form of hyperbolic partial differential equations; the two families of characteristics, referred to as α and β lines, correspond, respectively, to slip directions and slip plane normals in the case of anisotropic slip line theory applied to single crystals. More details about anisotropic slip line theory can be found in [Rice 1973] and [Kysar et al. 2005].

6. Analytic treatment of deformation and stress field

6.1. Gaussian pressure distribution on a (110) crystallographic orientation. The stress and deformation states associated with a Gaussian pressure loading are derived by assuming that the pressure is applied by a punch with a nonuniform pressure distribution. By this formulation, flat punch kinematics is employed, but the distribution of the stresses under the punch is deformed by a Gaussian distribution. The stress state in the triangular region immediately below the punch is at yield for both problems. Under these conditions, one expects there to be a singular point associated with the edges of the punch about which exist constant stress angular sectors. The only ambiguity in the derivation is to determine the precise positions of the singular points relative to the Gaussian pressure distribution. Therefore, the following procedure is employed to determine a scaling relationship for the positions of the singular points, and a detailed numerical simulation is performed to locate the precise position. The derivation for the (1 $\bar{1}$ 4) case can be found in [Wang et al. 2008].

We first assume that a uniaxial stress state consisting of uniform pressure, P^* , is applied to the surface to be shocked such that plastic deformation is incipient. Schmid's law for a plane strain deformation state with effective in-plane slip systems can be expressed as [Kysar et al. 2005]

$$\sigma_{12} = \tan \phi^{(\alpha)} \left(\frac{\sigma_{11} - \sigma_{22}}{2} \right) \pm \frac{\beta^{(\alpha)} \tau^{(\alpha)}}{\cos 2\phi^{(\alpha)}}, \quad (6)$$

where the superscript α denotes the active slip system, $\phi^{(\alpha)}$ represents the angle between the slip system and the x_1 -axis, $\tau^{(\alpha)}$ is the critical resolved shear stress which can be experimentally determined, and $\beta^{(\alpha)}$ is a geometric ratio ($\beta^{(1)} = \beta^{(3)} = 2/\sqrt{3}$, $\beta^{(2)} = \sqrt{3}$), defined by [Rice 1987]. As seen in Figure 1, for both cases considered, there are three effective slip systems denoted by i , ii , and iii , which can be activated, as in Table 1. In order to find a scaling relation for the approximate position of the singular point, we find the uniaxial stress at which plastic deformation initiates by solving (6) for P^* with $\sigma_{22} = -P^*$, $\sigma_{12} = 0$ and $\sigma_{11} = 0$ to obtain

$$P^* = \pm \frac{2\beta^{(\alpha)} \tau^{(\alpha)}}{\sin 2\phi^{(\alpha)}} \quad (7)$$

as the approximate pressure at which plastic deformation will initiate. This value of P^* is equated to $P(x)$ in (1), and the corresponding value of x , denoted as x_p , is

$$x_p = R \sqrt{\ln \frac{P_0^2 \sin^2 \phi}{(2\beta\tau)^2}}. \quad (8)$$

This result is a scaling relation for the approximate position of the singular point. We further define $x'_p = cx_p$, where c is a dimensionless constant of order unity to be determined by detailed numerical simulation to specify the precise location, x'_p , of the singular point.

Active slip system	ϕ for (110) case	ϕ for ($\bar{1}\bar{1}4$) case	β
<i>i</i>	144.7°	35.3°	$2/\sqrt{3}$
<i>ii</i>	90.0°	160.5°	$\sqrt{3}$
<i>iii</i>	35.3°	105.8°	$2/\sqrt{3}$

Table 1. Values of ϕ and β for active slip systems.

6.2. Analytic prediction of slip sectors for (110) and ($\bar{1}\bar{1}4$) orientations. For a Gaussian pressure distribution applied to the (110) surface, the surface tractions are given by $\sigma_{22} = -P(x)$ and $\sigma_{12} = 0$. If one assumes incipient plastic deformation, it is evident that the stress state will coincide with vertex *F* of the yield locus in Figure 2, left (see also Table 2 on page 97), so that both slip systems *i* and *iii* are activated under the pressure loading. From (7), the values of P^* for the slip systems *i* and *iii* are

$$(P^*)^i = \mp \frac{2\beta^{(1)}\tau^{(1)}}{\sin 2\phi^{(1)}}, \quad (P^*)^{iii} = \mp \frac{2\beta^{(3)}\tau^{(3)}}{\sin 2\phi^{(3)}},$$

where the superscripts on P^* denote the active slip system. Since $\phi^{(3)} = -\phi^{(1)}$, as indicated in Figure 2, we have $|P_*^{(1)}| = |P_*^{(3)}|$ so that both slip systems *i* and *iii* are expected to be activated under the Gaussian pressure distribution on the (110) surface, as expected. The approximate punch radius can then be estimated for the (110) orientation from (8) based upon the values of ϕ_1 and β_1 in Table 1.

The slip line field is then constructed based upon the concepts of [Rice 1973; 1987], as shown in Figure 3. There are constant stress angular sectors centered at each of the singular points; the boundaries of these sectors are slip directions and slip normals which pass through the singular point. In addition,

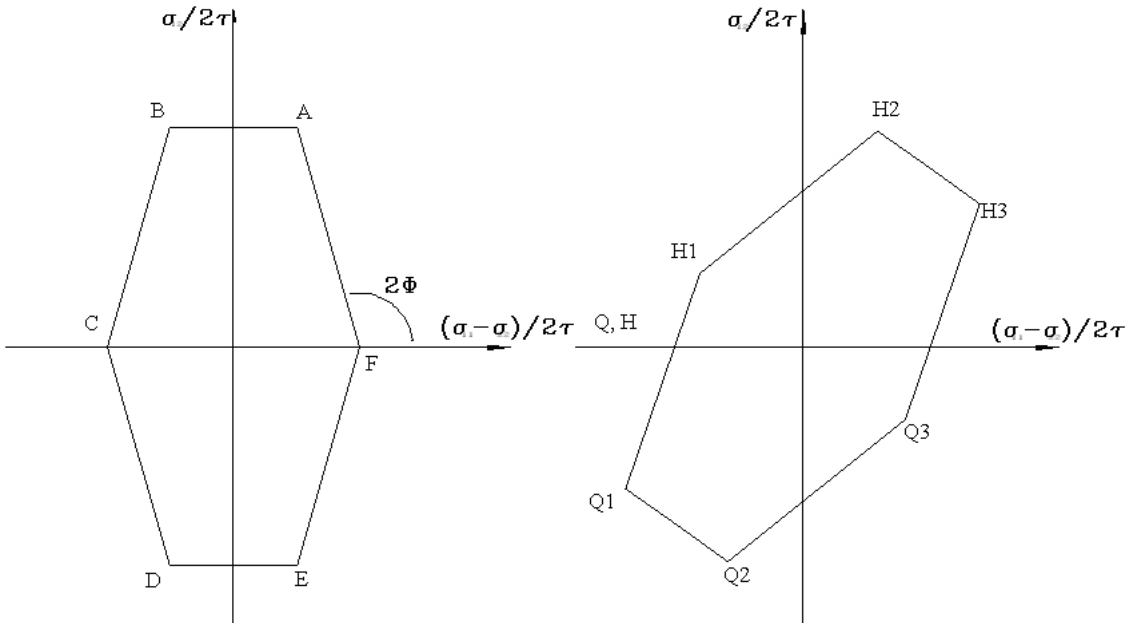


Figure 2. Yield locus for the (110) orientation (left) and for the ($\bar{1}\bar{1}4$) orientation (right).

there are constant stress triangular regions at the periphery of the slip line field. Within the center triangular region, the stress state corresponds to position F on the yield locus in Figure 2, right. From Figure 3, top it can be seen that the symmetric yield locus gives rise to a symmetric slip line field. On the other hand, the slip line field on the $(1\bar{1}4)$ surface, shown in Figure 3, bottom, as constructed by Wang et al. [2008] is asymmetric, reflecting the asymmetry of the yield locus for that orientation in Figure 2, right. From both parts of Figure 3, the geometry of the slip line field also provides an estimate for the

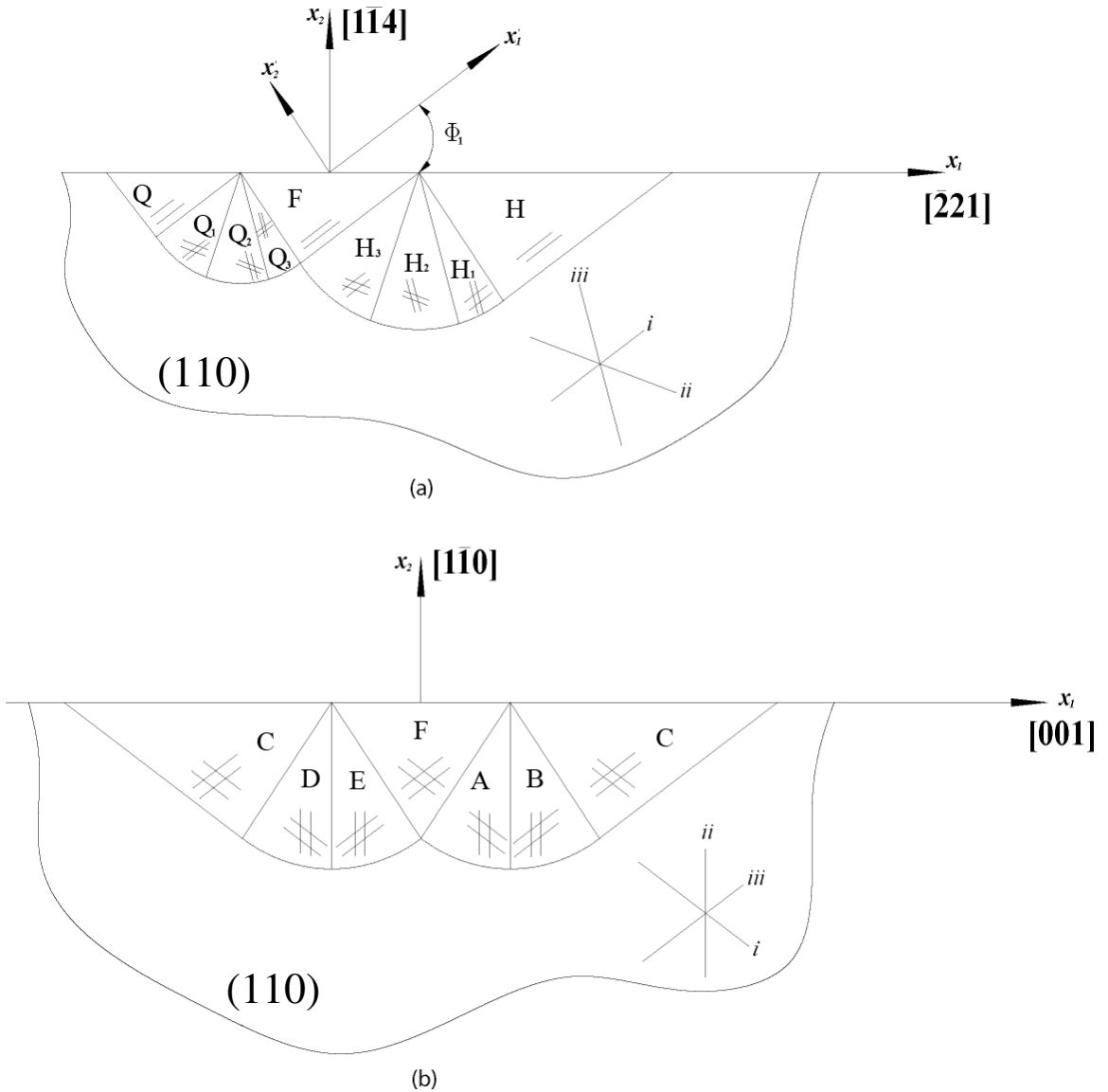


Figure 3. Geometry of slip line field under Gaussian loading for the $(1\bar{1}4)$ orientation (top) and the (110) orientation (bottom).

Vertex	$(\sigma_{11} + \sigma_{22})/2\tau$	σ_{12}/τ	Vertex	$(\sigma_{11} + \sigma_{22})/2\tau$	σ_{12}/τ
A	$\frac{1}{2}\sqrt{\frac{3}{2}}$	$\sqrt{3}$	H ₁	$-\frac{7}{8}\sqrt{6}$	$\frac{4}{9}\sqrt{3}$
B	$-\frac{1}{2}\sqrt{\frac{3}{2}}$	$\sqrt{3}$	H ₂	$\frac{1}{4}\sqrt{6}$	$\sqrt{3}$
C	$-\sqrt{\frac{3}{2}}$	0	H ₃	$\frac{23}{36}\sqrt{6}$	$\frac{5}{9}\sqrt{3}$
D	$-\frac{1}{2}\sqrt{\frac{3}{2}}$	$-\sqrt{3}$	F	$\frac{1}{2}\sqrt{6}$	0
E	$\frac{1}{2}\sqrt{\frac{3}{2}}$	$-\sqrt{3}$	Q ₃	$\frac{7}{18}\sqrt{6}$	$-\frac{4}{9}\sqrt{3}$
F	$\sqrt{\frac{3}{2}}$	0	Q ₂	$-\frac{1}{4}\sqrt{6}$	$-\sqrt{3}$
			Q ₁	$-\frac{23}{36}\sqrt{6}$	$-\frac{5}{9}\sqrt{3}$
			Q	$-\frac{1}{2}\sqrt{6}$	0

Table 2. Yield locus vertices for the (110) case (left) and the (1 $\bar{1}$ 4) case (right).

size of the plastically deformed region for the (110) and (1 $\bar{1}$ 4) cases, respectively:

$$L = 2x_p \left(1 + \frac{1}{\cos^2 \phi}\right) = 2cR \sqrt{\ln \frac{P_0^2 \sin^2 \phi}{(2\beta\theta)^2}} \left(1 + \frac{1}{\cos^2 \phi}\right), \quad (9)$$

$$L = 2x_p (1 + \cot \phi + \tan \phi) = 2\sqrt{2}cR (1 + \cot \phi + \tan \phi) \sqrt{\ln \left(\frac{P_0}{2A}\right) + \ln \sin 2\phi}.$$

6.3. Analytic prediction of stresses within slip systems. Rice [1987] derived for the asymptotic deformation and stress fields under plane strain conditions in elastic-ideally plastic single crystals. By satisfying equilibrium and assuming that a particular angular sector is at yield, he showed that as $r \rightarrow 0$ the stress state must be of a “constant stress type”. Furthermore, since the stress states along the crack flanks and the prolongation of the crack are different, the stress field has to be divided into several constant stress sectors separated by either elastic sectors or lines of discontinuity. For the case of a stationary crack, if the entire domain is at yield, the stress state will necessarily follow the yield locus in stress space; each vertex corresponds to the stress state in a constant angle sector. In the transition region between sectors there is a discontinuity corresponding to the edge on the yield locus which connects two adjacent vertices. These stress discontinuities are constrained to lie at certain angles and coincide with families of slip lines and slip plane normals. Rice [1982] stated that an analogous approach can be used for punch problems. The analytic prediction of the stress distribution under a Gaussian pressure distribution based on anisotropic slip line theory in aluminum with (1 $\bar{1}$ 4) orientation is discussed in detail in [Wang et al. 2008]. Although the (110) orientation is more complex because of double slip, a similar conclusion about stress distribution can be drawn for it; see [Rice 1987].

The solution can be derived by assuming a Gaussian pressure distribution for $x \leq x'_p$, and zero traction boundary conditions for $x > x'_p$. Then, following established procedures [Rice 1973; 1987; Wang et al. 2008], the relationship between the change of average stress $\Delta\sigma = \frac{1}{2}\Delta(\sigma_{11} + \sigma_{22})$ and arc length ΔL , which has units of stress, around the yield locus is

$$\frac{1}{2}\Delta(\sigma_{11} + \sigma_{22}) = -\Delta L. \quad (10)$$

Sector	σ_{11}/τ_{cr}	σ_{22}/τ_{cr}	σ_{12}/τ_{cr}	Active slip systems
A	$-\frac{3}{2}\sqrt{6}$	$-2\sqrt{6}$	$\sqrt{3}$	<i>i, ii</i>
B	$-\frac{3}{2}\sqrt{6}$	$-\sqrt{6}$	$\sqrt{3}$	<i>ii, iii</i>
C	$-\sqrt{6}$	0	0	<i>i, iii</i>
D	$-\frac{3}{2}\sqrt{6}$	$-\sqrt{6}$	$-\sqrt{3}$	<i>i, ii</i>
E	$-\frac{3}{2}\sqrt{6}$	$-2\sqrt{6}$	$-\sqrt{3}$	<i>ii, iii</i>

Sector	σ_{11}/τ_{cr}	σ_{22}/τ_{cr}	σ_{12}/τ_{cr}	Active slip systems
H	$-\sqrt{6}$	0	0	<i>i</i>
H ₁	$-\frac{11}{9}\sqrt{6}$	$-\frac{4}{9}\sqrt{6}$	$\frac{4}{9}\sqrt{3}$	<i>i, iii</i>
H ₂	$-\frac{4}{3}\sqrt{6}$	$-\frac{11}{6}\sqrt{6}$	$\sqrt{3}$	<i>ii, iii</i>
H ₃	$-\frac{13}{9}\sqrt{6}$	$-\frac{49}{18}\sqrt{6}$	$\frac{5}{9}\sqrt{3}$	<i>i, ii</i>
Q ₃	$-\frac{16}{9}\sqrt{6}$	$-\frac{23}{9}\sqrt{6}$	$-\frac{4}{9}\sqrt{3}$	<i>i, iii</i>
Q ₂	$-\frac{5}{3}\sqrt{6}$	$-\frac{7}{6}\sqrt{6}$	$-\sqrt{3}$	<i>ii, iii</i>
Q ₁	$-\frac{14}{9}\sqrt{6}$	$-\frac{5}{18}\sqrt{6}$	$-\frac{5}{9}\sqrt{3}$	<i>i, ii</i>
Q	$-\sqrt{6}$	0	0	<i>i</i>

Table 3. Stresses within sectors for the (110) case (top) and the (1 $\bar{1}$ 4) case (bottom).

Yield locus vertices can be found from geometry, and thus the arc length L can be calculated so that stresses in each of the regions in Figure 3 can be derived. Table 3 shows the normalized values of stress components in each sector for both the (110) and (1 $\bar{1}$ 4) case. More detailed solutions for cracks and cylindrical voids in single crystals case can be found in [Rice 1987; Kysar et al. 2005].

6.4. Analytic prediction of lattice rotation for (110) and (1 $\bar{1}$ 4) orientations. As seen in Section 4, the spin tensor Ω consists of Ω^* , which corresponds to lattice rotation, and Ω^P , associated with plastic slip. Following [Asaro 1983], the plastic part of Ω^P is

$$\Omega^P = \sum_{\alpha=1}^N W^{(\alpha)} \cdot \dot{\lambda}^\alpha, \quad (11)$$

where α represents active slip systems, $\dot{\gamma}$ is the rate of shear, and the tensor W is defined by

$$W^{(\alpha)} = \frac{1}{2}(s^{(\alpha)} \otimes n^{(\alpha)} - n^{(\alpha)} \otimes s^{(\alpha)}). \quad (12)$$

Therefore, Ω^* can be rewritten as

$$\Omega^* = \Omega - \frac{1}{2} \sum_{\alpha=1}^N \dot{\gamma} (s^{(\alpha)} \otimes n^{(\alpha)} - n^{(\alpha)} \otimes s^{(\alpha)}) \quad (13)$$

which gives a relation between the spin tensor responsible for lattice rotation and the slip rate of each active slip system. If \mathbf{n} and \mathbf{s} are projected onto the x_1, x_2 plane and rescaled as unit vectors \mathbf{N} and \mathbf{S} , taking into account the plane strain condition, (8) can be expressed as

$$\Omega^* = \Omega - \frac{1}{2} \sum_{\alpha=1}^N \dot{\gamma} (S^{(\alpha)} \otimes N^{(\alpha)} - N^{(\alpha)} \otimes S^{(\alpha)}) \beta^{(\alpha)} \quad (14)$$

From [Rice 1987] it follows that $S_1 = N_2, S_2 = -N_1$, so the term in parentheses reduces to a constant. The only factors left under the summation are the strain rate and the β term, which is different for each slip system, as discussed by Rice.

Unlike the (1 $\bar{1}$ 4) case, in which only one slip system is active in the triangular regions, in the (110) orientation there are two active slip systems. From the solution for the stresses, it can be shown that the shear strain on each slip system has the same sign, so that the lattice spin induced by both slip systems also has the same sign, which leads to the conclusion that the deformation associated with each slip system adds to the total rotation. Furthermore, the (110) orientation is symmetric, and therefore each active slip system equally contributes to the magnitude of the lattice deformation. On the other hand, only one slip system is active for the (1 $\bar{1}$ 4) case, which suggests that the overall lattice rotation might be less than that in the symmetric case. A more detailed discussion about the numerical and experimental results is given below.

7. Numerical results and comparison with experiments and analytic solutions

7.1. Slip sectors and shear strain increments. According to the analytic solution, the entire deformation field is divided into sectors. In each of those sectors one or two slips are active. As discussed by [Rice 1987], boundaries of sectors are slip directions and slip normals which represent lines of stress discontinuity. The numerical model agrees well with the analytic solution as shown by [Wang et al. 2008] for (1 $\bar{1}$ 4) case. In the case of the (110) orientation, the analytic results derived in the previous section and superimposed on the numerical findings are in good agreement as well, as seen in Figure 4. However, here, emphasis is placed on comparison between the deformation states of the symmetric and asymmetric orientations. Both total shear as well as shear increments for each slip system are of interest. Figure 4 depicts antisymmetry of shear strain increments associated with slips i and iii . At the same time, shear strain increment on slip system ii is symmetric about the center of the shock. The extent of the shear strain increment of all slip systems agrees well with the deformation field derived analytically, if one chooses the consistent c to determine x'_p . Likewise, the (1 $\bar{1}$ 4) calculations agree well with the analytic solution (see Figure 5). The distribution of the shear strain increments is larger on the right side of the deformation field.

7.2. Lattice rotation. Plastic deformation induced by μ LSP causes crystallographic lattice rotation that was characterized via Electron Backscatter Diffraction (EBSD). The region of interest is mapped after laser treatment and its crystallographic orientation compared with the known initial state which serves as a reference. More details about this method can be found in [Kysar and Briant 2002]. Results shown here were reported elsewhere [Wang et al. 2008; Vukelic et al. \geq 2009], and in this study they serve as a comparison with the numerical model.

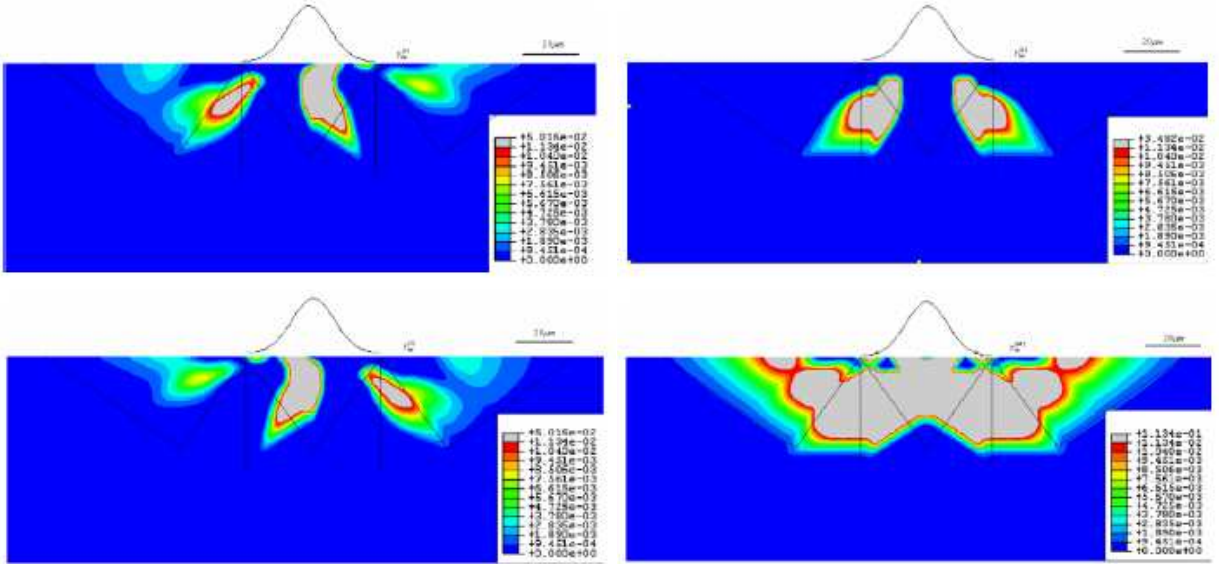


Figure 4. Shear strain increment in each slip system at the end of the loading step for the (110) orientation. Top left, increment in slip system i ; top right, slip system ii ; bottom left, slip system iii ; bottom right, total shear strain increment.

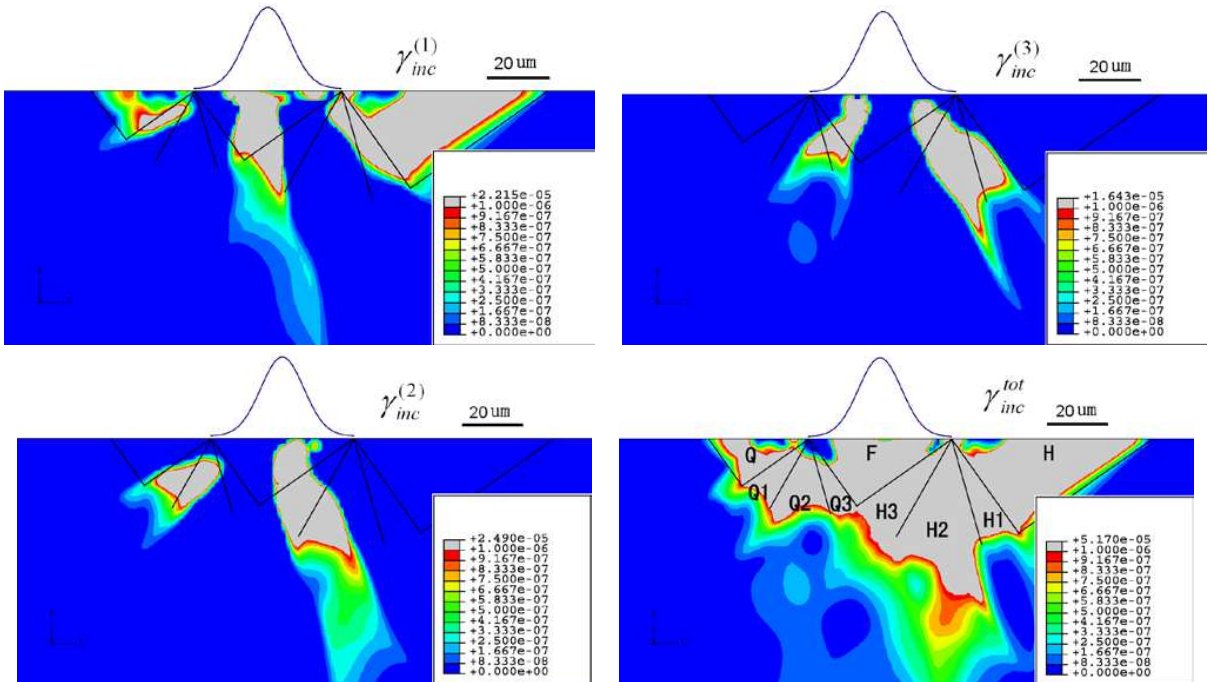


Figure 5. Shear strain increment in each slip system in the end of loading step for (114) orientation. Top left, increment in slip system i ; top right, slip system ii ; bottom left, slip system iii ; bottom right, total shear strain increment.

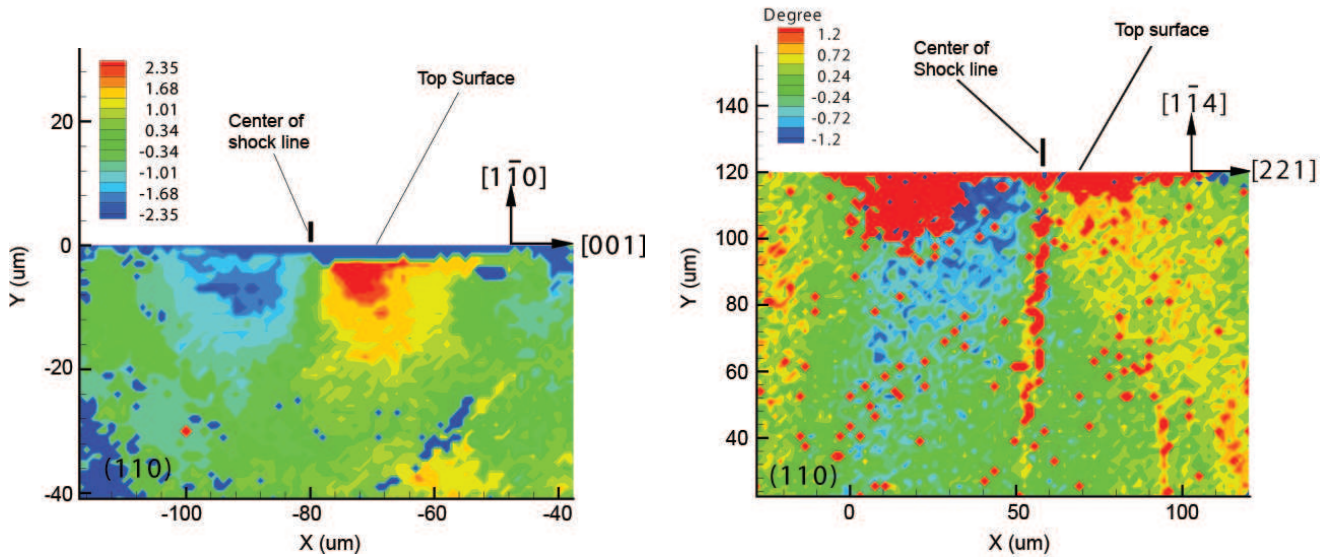


Figure 6. Lattice rotation contour map on the (110) cross section. Positive rotation is counterclockwise about the z -axis.

Lattice rotation results obtained from EBSD measurements of the cross-section are shown in Figure 6. Antisymmetric rotation about the center of the shock line can be observed with blue regions corresponding to counterclockwise rotation and red regions depicting clockwise rotation. Green areas in the field represent unrotated parts of the crystal. From Figure 6a it can be seen that deformation of the (110) crystal is approximately symmetric and slightly narrower than in the (114) case. The magnitude of deformation is largest close to the surface of the specimen and about 15 μm away from the center of the shock line. It can also be seen that directly under the center of the shock line is a region of unrotated crystal. The magnitude of deformation is different for the symmetric and asymmetric cases; for the (110) orientation, the lattice rotates between $\pm 2.4^\circ$, almost double of the rotation of the (114) orientation which is about $\pm 1.2^\circ$. These results are consistent with analytic predictions derived in the previous section that the double slip will cause a larger increase in the lattice rotation than the case of a single slip corresponding to the (114) orientation.

Numerical results of the in-plane lattice rotation are shown in Figure 7. One sees there good agreement between simulation and experimental findings. The main trend for the case of counterclockwise and clockwise rotations located directly under the center of the loading is apparent. The (110) orientation gives a symmetric response as opposed to the asymmetric case of (114). Also, the magnitude of the lattice rotation is larger for the double slip case. However, there is a discrepancy between experimental results and simulation, mainly seen in the magnitude of rotation. This arises from the limitations of the FEM model in which the effects of inertia and work hardening are being neglected.

7.3. Stress distribution. The FEM results of residual stress, σ_{11} , after unloading are shown in Figure 8. It can be seen that the stress field is symmetric in the (110) case and asymmetric in the (114) case. A region of compressive residual stress exists in the center region, whereas self-equilibrating regions of

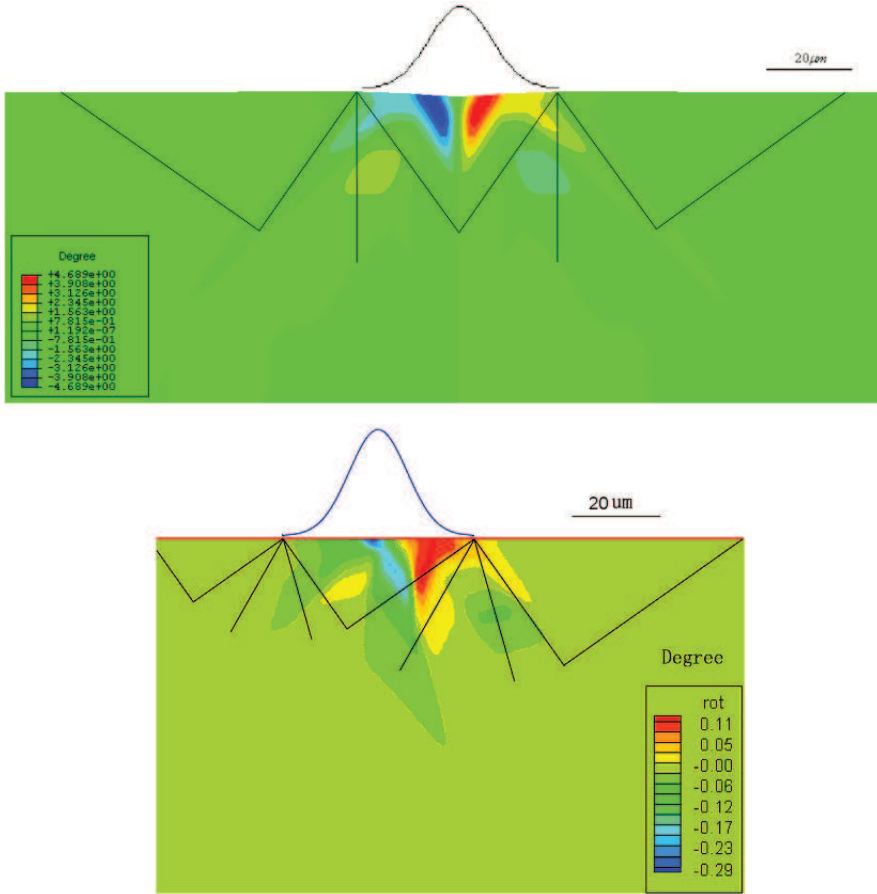


Figure 7. Lattice deformation contour by FEM for the (110) orientation (top) and the (114) orientation (bottom).

tensile residual stress is located far from the center, with the exception of two small regions of tensile residual stress located at the tips of the assumed ends of the punch. The trend shown in Figure 8 suggests that the process of μ LSP is beneficial to the fatigue life and wear resistance of micro components experiencing cyclic loading. Also, it should be noted that in previous studies [Wang et al. 2008], the surface displacement after applying laser shocks onto the top surface has been measured by atomic force microscopy (AFM) and optical profilometry [Vukelic et al. \geq 2009], and the trend coincides with the results captured by finite element simulation.

8. Conclusion

We presented a comparison between laser shock peening of two different orientations of aluminum single crystals, one symmetric and one asymmetric. Anisotropic slip line theory was employed for the construction of slip line fields for both orientations and compared with numerical results. In addition, the stress distribution in angular sectors has been calculated. For the double slip symmetric case, plastic deformation caused by two slip systems adds to the total deformation as characterized by the lattice rotations

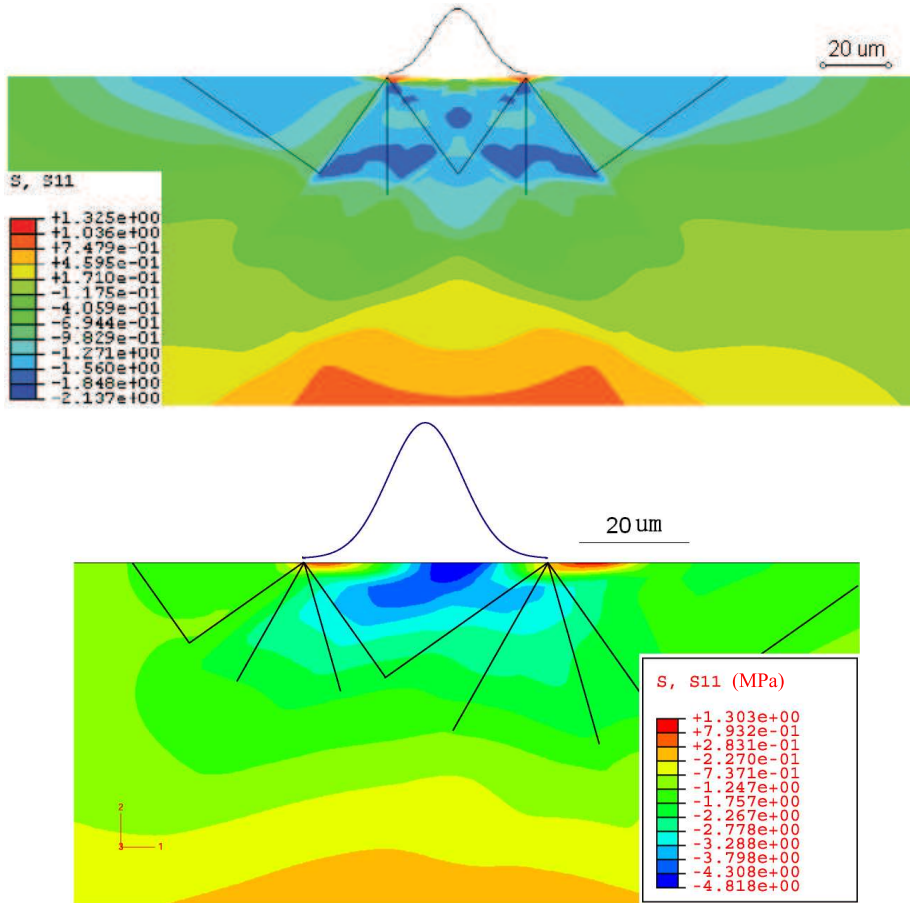


Figure 8. FEM simulation of residual stress distribution for the (110) orientation (top) and the $(1\bar{1}4)$ orientation (bottom).

which suggests that deformation in the symmetric orientation will be greater than in the asymmetric case. A numerical model is established for a more detailed investigation of the μ LSP process and compared to experiments. Experimental measurement of lattice rotation via EBSD in the double slip case shows that lattice rotation is twice as large as in the single slip case, which is consistent with the analytic work. Future work will include the effect of heterogeneity through the study of the grain boundary response to μ LSP, which will be achieved by examination of bicrystals.

References

- [Asaro 1983] R. J. Asaro, “Micromechanics of crystals and polycrystals”, *Adv. Appl. Mech.* **23** (1983), 1–115.
- [Booker and Davis 1972] J. R. Booker and E. H. Davis, “A general treatment of plastic anisotropy under conditions of plane strain”, *J. Mech. Phys. Solids* **20**:4 (1972), 239–250.
- [Chen et al. 2004a] H. Q. Chen, J. W. Kysar, and Y. L. Yao, “Characterization of plastic deformation induced by microscale laser shock peening”, *J. Appl. Mech. (ASME)* **71**:5 (2004), 713–723.

- [Chen et al. 2004b] H. Q. Chen, Y. L. Yao, and J. W. Kysar, “Spatially resolved characterization of residual stress induced by micro scale laser shock peening”, *J. Manuf. Sci. Eng. (ASME)* **126**:2 (2004), 226–236.
- [Clauer and Holbrook 1981] A. H. Clauer and J. H. Holbrook, “Effects of laser induced shock waves on metals”, Chapter 38, pp. 675–703 in *Shock waves and high-strain-rate phenomena in metals: concepts and applications* (Albuquerque, NM, 1980), edited by M. A. Meyers and L. E. Murr, Plenum, New York, 1981.
- [Clauer and Lahrman 2001] A. H. Clauer and D. F. Lahrman, “Laser shock processing as a surface enhancement process”, *Key Eng. Mat.* **197** (2001), 121–142.
- [Crone et al. 2004] W. C. Crone, T. W. Shield, A. Creuziger, and B. Henneman, “Orientation dependence of the plastic slip near notches in ductile FCC single crystals”, *J. Mech. Phys. Solids* **52**:1 (2004), 85–112.
- [Drugan 2001] W. J. Drugan, “Asymptotic solutions for tensile crack tip fields without kink-type shear bands in elastic-ideally plastic single crystals”, *J. Mech. Phys. Solids* **49**:9 (2001), 2155–2176.
- [Fabbro et al. 1990] R. Fabbro, J. Fournier, P. Ballard, and D. Devaux, “Physical study of laser-produced plasma in confined geometry”, *J. Appl. Phys.* **68**:2 (1990), 775–784.
- [Fan et al. 2005] Y. Fan, Y. Wang, S. Vukelic, and Y. L. Yao, “Wave-solid interactions in laser-shock-induced deformation processes”, *J. Appl. Phys.* **98**:10 (2005), 104904–104904–11.
- [Hammersley et al. 2000] G. Hammersley, L. A. Hackel, and F. Harris, “Surface prestressing to improve fatigue strength of components by laser shot peening”, *Opt. Lasers Eng.* **34**:4–6 (2000), 327–337.
- [Hencky 1923] H. Hencky, “Über einige statisch bestimmte Fälle des Gleichgewichts in plastischen Körpern”, *Z. Angew. Math. Mech.* **3**:4 (1923), 241–251.
- [Hill 1998] R. Hill, *The mathematical theory of plasticity*, Oxford University Press, New York, 1998.
- [Huang 1991] Y. Huang, “A user-material subroutine incorporating single crystal plasticity in the ABAQUS finite element program”, Division of Applied Sciences, Harvard University, Cambridge, MA, 1991, Available at http://www.columbia.edu/~jk2079/fem/umat_documentation.pdf.
- [Kysar 1997] J. W. Kysar, “Addendum to ‘A user-material subroutine incorporating single crystal plasticity in the ABAQUS finite element program, Mech Report 178’”, Division of Applied Sciences, Harvard University, Cambridge, MA, 1997, Available at <http://www.columbia.edu/~jk2079/fem/Addendum%20to%20umat.pdf>.
- [Kysar 2001a] J. W. Kysar, “Continuum simulations of directional dependence of crack growth along a copper/sapphire bicrystal interface, I: Experiments and crystal plasticity background”, *J. Mech. Phys. Solids* **49**:5 (2001), 1099–1128.
- [Kysar 2001b] J. W. Kysar, “Continuum simulations of directional dependence of crack growth along a copper/sapphire bicrystal interface, II: Crack tip stress/deformation analysis”, *J. Mech. Phys. Solids* **49**:5 (2001), 1129–1153.
- [Kysar and Briant 2002] J. W. Kysar and C. L. Briant, “Crack tip deformation fields in ductile single crystals”, *Acta Mater.* **50**:9 (2002), 2367–2380.
- [Kysar et al. 2005] J. W. Kysar, Y. X. Gan, and G. Mendez-Arzuza, “Cylindrical void in a rigid-ideally plastic single crystal, I: Anisotropic slip line theory solution for face-centered cubic crystals”, *Int. J. Plast.* **21**:8 (2005), 1481–1520.
- [Prandtl 1923] L. Prandtl, “Anwendungsbeispiele zu einem Henckyschen Satz über das plastische Gleichgewicht”, *Z. Angew. Math. Mech.* **3**:6 (1923), 401–406.
- [Rice 1973] J. R. Rice, “Plane strain slip line theory for anisotropic rigid/plastic materials”, *J. Mech. Phys. Solids* **21**:2 (1973), 63–74.
- [Rice 1982] J. R. Rice, “Elastic-plastic crack growth”, pp. 539–562 in *Mechanics of solids: The Rodney Hill 60th anniversary volume*, edited by H. G. Hopkins and M. J. Sewell, Pergamon, Oxford, 1982.
- [Rice 1987] J. R. Rice, “Tensile crack tip fields in elastic-ideally plastic crystals”, *Mech. Mater.* **6**:4 (1987), 317–335.
- [Vukelic et al. ≥ 2009] S. Vukelic, Y. Wang, J. W. Kysar, and Y. L. Yao, “Dynamic material response of aluminum single crystal under micro scale laser shock peening”. Submitted to *J. Manuf. Sci. Eng. (ASME)*.
- [Wang et al. 2008] Y. Wang, J. W. Kysar, and Y. L. Yao, “Analytical solution of anisotropic plastic deformation induced by micro-scale laser shock peening”, *Mech. Mater.* **40**:3 (2008), 100–114.
- [Zhang and Yao 2002] W. Zhang and Y. L. Yao, “Microscale laser shock processing of metallic components”, *J. Manuf. Sci. Eng. (ASME)* **124**:2 (2002), 369–378.

Received 17 Sep 2008. Revised 10 Nov 2008. Accepted 13 Nov 2008.

SINIŠA VUKELIĆ: sv2147@columbia.edu

Columbia University, Mechanical Engineering Department, 500 W 120th Street, S. W. Mudd Building Room 220, MC 4703, New York, NY 10027, United States

YOUNENG WANG: yw2119@columbia.edu

Columbia University, Mechanical Engineering Department, 500 W 120th Street, S. W. Mudd Building Room 220, MC 4703, New York, NY 10027, United States

JEFFREY W. KYSAR: jk2079@columbia.edu

Columbia University, Mechanical Engineering Department, 500 W 120th Street, S. W. Mudd Building Room 220, MC 4703, New York, NY 10027, United States

Y. LAWRENCE YAO: yly1@columbia.edu

Columbia University, Mechanical Engineering Department, 500 W 120th Street, S. W. Mudd Building Room 220, MC 4703, New York, NY 10027, United States